Optofluidic Near-Field Optical Microscopy: Near-Field Mapping of a Silicon Nanocavity Using Trapped Microbeads

Christophe Pin,[†,‡,§,∥] Benoît Cluzel,*[,†] Claude Renaut,[†,‡,§,∥,⊥] Emmanuel Picard,[‡,§] David Peyrade,[∥] Emmanuel Hadji,[‡,§] and Frédérique de Fornel[†]

[†]Groupe Optique de Champ Proche - LRC SiNOPTIQ du CEA n°DSM-08-36, Laboratoire Interdisciplinaire Carnot de Bourgogne UMR CNRS 6303, Université de Bourgogne-Franche Comté, 9. Av. A. Savary, 21078 Dijon, France

[‡]Université Grenoble Alpes, INAC-SP2M-SINAPS, F-38000 Grenoble, France

[§]CEA, INAC-SP2M-SINAPS, F-38000 Grenoble, France

[∥] Université Grenoble Alpes, CNRS, CEA-Leti Minatec, LTM, F-38054 Grenoble Cedex, France

S *Supporting Information*

ABSTRACT: By analyzing the thermal motion of fluorescent dielectric microbeads trapped in the near-field of a silicon nanocavity, we investigate the influence of the bead's size and the trapping laser power on the shape of the optical trap and the "effective" trap stiffness. We demonstrate that the trapping potential is proportional to the subwavelength patterns of the electromagnetic near-field intensity distribution for unexpectedly large Mie particle sizes. More especially, we show that mapping the trapping potential experienced by a 500 nm diameter bead reveals the nanopatterns of the cavity resonant mode. This result highlights how photonic force microscopy in nanotweezers can provide an elegant way to image evanescent fields at the nanoscale via the thermal motion of optically trapped fluorescent microprobes.

KEYWORDS: *photonic crystal, optical tweezers, near-field optical forces, photonic force microscopy, optical lattice, near-field optical microscopy*
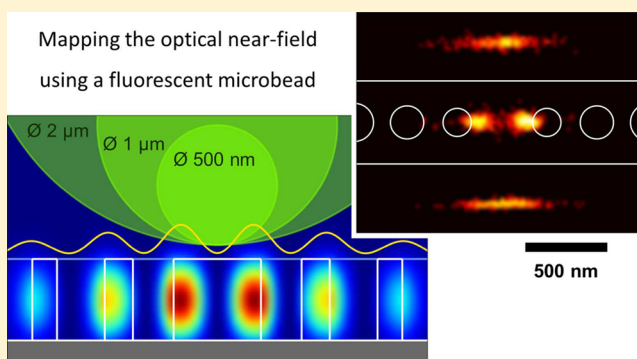
O ptical forces that rely on the mechanical interactions between light and matter were first used to trap microparticles by A. Ashkin in 1970.[1] Since then, optical trapping has enabled countless applications in physics, chemistry, and biology. This success is mostly based on the widespread use of single-beam gradient-force optical traps, better known as optical tweezers, which allow for noninvasive three-dimensional optical manipulation and force measurements on microscopic objects with unrivalled precision.[2,3]

More recently, following the pioneering work of Kawata and Tani,[4] near-field optical forces arising from evanescent waves at the interface of light confining structures have attracted a growing interest.[5,6] In particular, near-field photonic[5−17] and plasmonic[5,18−25] nanotweezers, in which subdiffraction-limit light confinement is achieved, have shown promising capabilities for lab-on-chip applications such as trapping,[7−12,19−21] manipulation,[13,14,22,23] sensing,[15−17] protein unfolding,[24] or even DNA hairpin unzipping[25] at low power levels.

In the same way that far-field optical tweezers have to be calibrated by analyzing the trapped objects dynamics to achieve stable particle manipulation and precise force measurements,[2,26−28] it is of prime importance to experimentally

determine nanotweezers' trapping potential. However, unlike their far-field counterparts, nanotweezers rely on electromagnetic modes confined in, or near, nanostructures, leading to non-Gaussian optical traps with complex shapes.[7,13,18,21,23] Besides, objects trapped in the near-field of those nanostructures interact with both the local electromagnetic and electrostatic fields[29] and can also experience additional local heating and convective forces, especially in the case of plasmonic nanotweezers.[5,18,21] For these reasons, the resulting trapping potential appears very sensitive not only to the nanoscale features of the nanotweezers and their near-field, but also to the properties of the trapped object itself, such as its size, shape, or material, to such an extent that defining an "effective" trap stiffness becomes sometimes difficult, if not impossible.[21]

In this paper, we provide a detailed description of the trapping potential experienced by fluorescent polystyrene microbeads used as Brownian probes to investigate optical forces in the near-field of a silicon photonic crystal nanocavity. By analyzing the thermal motion of trapped microbeads, we
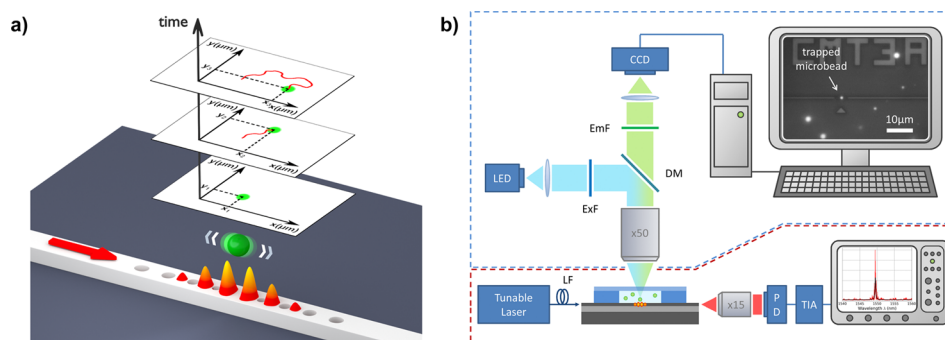
Figure 1. (a) Schematic representation of a fluorescent microbead optically trapped in the near-field of a nanobeam cavity. Fluorescence of the bead allows for the thermal agitation of the bead to be accurately observed and recorded over the time. (b) Schematic of the experimental setup that combines an end-fire coupling optical bench at telecom wavelength (delimited by the red dashed line) to a homemade fluorescence microscope (delimited by the blue dashed line). Telecom light is coupled from a tunable fiber laser to a nanobeam waveguide using a polarization-maintaining lensed fiber (LF) and detected using a standard detection scheme with a photodiode (PD) and a trans-impedance amplifier (TIA) linked to an oscilloscope. The fluorescence excitation at 470 nm provided by a blue light emitting diode (LED) is separated from the fluorescence emission of the microbeads thanks to a dichroic mirror (DM) and a set of excitation and emission filters (ExF, EmF). A CCD camera is used to observe and record at 24 fps microscope images of the trapping events.
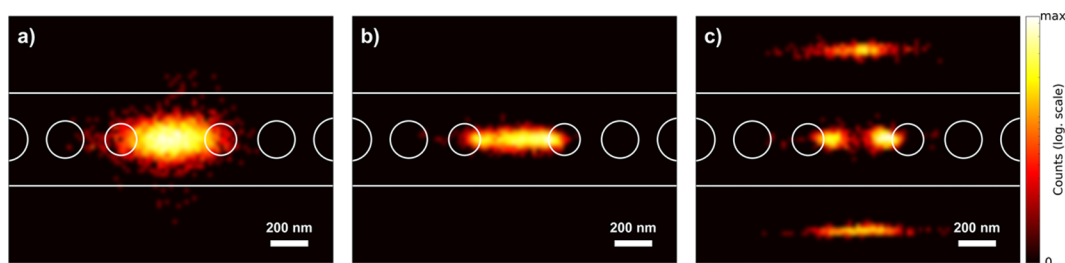

Figure 2. Experimental images of the trapping potential experienced, respectively, by a (a) 2 μm, (b) 1 μm, and (c) 500 nm microbead. These top-view images are obtained by mapping and plotting with a logarithmic color scale the position probability distribution of trapped microbeads.

explore the bead size-dependence of the trapping potential shape and the "effective" trap stiffness. When decreasing the bead's size from 2 μm to 500 nm in diameter, we observe a clear transition from an "averaged" trapping regime toward a "proportional" trapping regime. In light of the literature, it appears that this "size-effect" occurs here for unexpectedly large microbead's sizes.[30−38] We also analyze how a variation of the input laser power and, thus, of the depth of the potential well impacts the "effective" shape of the trap. In light of those results, we eventually discuss the concept of optofluidic near-field optical microscopy: an original approach to image evanescent fields at the nanoscale via the thermal motion of optically trapped fluorescent microprobes.

EXPERIMENTAL DETAILS

As represented in Figure 1a, the near-field photonic nano-tweezers used in this work consist of silicon nanobeam cavities.[39] Earlier works have proven their capability to efficiently trap objects with sizes ranging from a few nanometers[7,16] to a few micrometers[8,14] thanks to the optical gradient forces resulting from the strong light confinement achieved at resonance. The nanocavities are fabricated in 500 nm large silicon waveguides on a silicon-on-insulator (SOI) photonic chip made of a 340 nm thick silicon layer on a 2 μm thick oxide layer. A static microfluidic cell was then assembled on the photonic chip[8] and filled with an aqueous colloidal solution containing green fluorescent polystyrene microbeads of different sizes, respectively, 500 nm, 1 μm, and 2 μm in diameter. As shown on Figure 1b, these microbeads can be accurately observed with a standard microscope objective (50×,

NA: 0.75) mounted on a homemade fluorescence microscope, while the photonic chip is being operated at telecom wavelength.

Figure 1a also illustrates the fact that, when optically trapped, a microbead still experiences some agitation because of its thermal energy. The resulting motion of the bead is governed by Boltzmann statistics which links the probability of presence $P(r)$ of the particle with the trapping potential U_{trap} according to the following relation:

$$P(\mathbf{r}) \propto \exp\left(-\frac{U_{trap}}{k_B T}\right)$$

where k_B is the Boltzmann constant and T is the temperature.[2] Tracking the spatial distribution of the successive positions of a trapped microbead enables therefore to experimentally map the trapping potential landscape restraining the bead's motion.[40]

For each trapping event observed, videos of the trapped microbead's motion were recorded with a CCD camera, as shown in Figure 1b. The discretization step of the captured images was measured to be 42 nm per pixel. Working with a frame rate of 24 fps, an acquisition time of only a few minutes is long enough to obtain a sequence of a few thousands of images that can be used to build a valid statistical distribution of the trapped microbead's positions. The successive positions of the trapped microbead centroid were extracted from each image sequence using a particle tracking algorithm (Mosaic group's Particle Tracker plugin for ImageJ/Fiji).[41] The relatively large size of the fluorescent microbeads and the use of optical filters for fluorescence microscopy make it possible to get images with
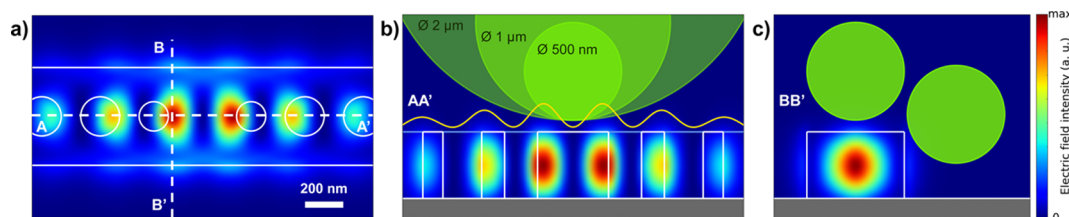
Figure 3. (a) Top view of the 3D Finite Difference Time Domain (FDTD) calculation of the electric field intensity 35 nm above the nanocavity surface. (b) AA′ and (c) BB′ cross sections of the calculated field intensity. Scaled representations of the microbeads and the near-field intensity profile are superimposed on the 3D FDTD simulation results.

a high signal-to-noise ratio, and thus to achieve subpixel localization of the trapped microbead centroid.[41] Two-dimensional histograms of these positions were then calculated with a grid of 0.5×0.5 pixel^2 unit surface areas, corresponding to 21 nm discretization steps. As a result, discretized maps of the position probability distribution $P(r)$ were obtained from the tracking of the microbeads' motion. Plotting them using a logarithmic color scale allows recreating experimental top-view images of the trapping potential experienced by each microbead.

■ RESULTS AND DISCUSSION

Figure 2 shows the trapping potentials measured for different microbead sizes, respectively, 2 μm (Figure 2a), 1 μm (Figure 2b), and 500 nm (Figure 2c) in diameter. All the results presented here were obtained on the same nanocavity and in the same experimental conditions. For comparison, the calculated electric near-field intensity of the cavity resonant mode, obtained from 3D Finite-Difference Time-Domain (FDTD) simulation, is shown on Figure 3a. In order to support the discussion, two orthogonal cross sections of the calculated resonant mode electric field intensity are also provided in Figure 3b,c, with scaled representations of the different microbeads.

The trapping potential of the 2 μm bead, shown in Figure 2a, exhibits a single potential well centered on the nanocavity. This potential well has a large elliptic shape covering the whole central area of the cavity. Since the trapped microbead volume overlaps a large part of the cavity near-field, as it can be seen on the field calculation shown in Figure 3b, several antinodes of the resonant mode contribute at the same time to the global trapping force applied on the bead. As a result, the 2 μm bead appears to be sensitive to the Gaussian envelope of the cavity resonant mode intensity rather than to each of the antinodes of the mode. The cross-section of the position probability distribution along the nanocavity axis, plotted in yellow on Figure 4, reveals a well-fitted Gaussian profile overlapping the two main antinodes of the resonant mode. Such a "size-effect", leading to the trapping of Mie microparticles on spots of minimal field intensity, has been already observed and reported in studies on optical lattices.[31−33] We refer here to this trapping regime as the "averaged" regime since the trapping potential results from the averaged contribution of different near-field optical traps. In terms of trapping efficiency, this "averaged" trapping regime leads to a rather loose trap, with stiffnesses $k_x = 0.24 \pm 0.01$ fN·nm^{-1} (along the nanocavity axis) and $k_y = 1.3 \pm 0.1$ fN·nm^{-1} (along the perpendicular direction).

As shown in Figure 2b, the trapping potential of the 1 μm bead has a more elongated shape joining the two main antinodes of the resonant mode. Whereas a better lateral confinement of the bead's motion is achieved ($k_y = 6.5 \pm 1.6$
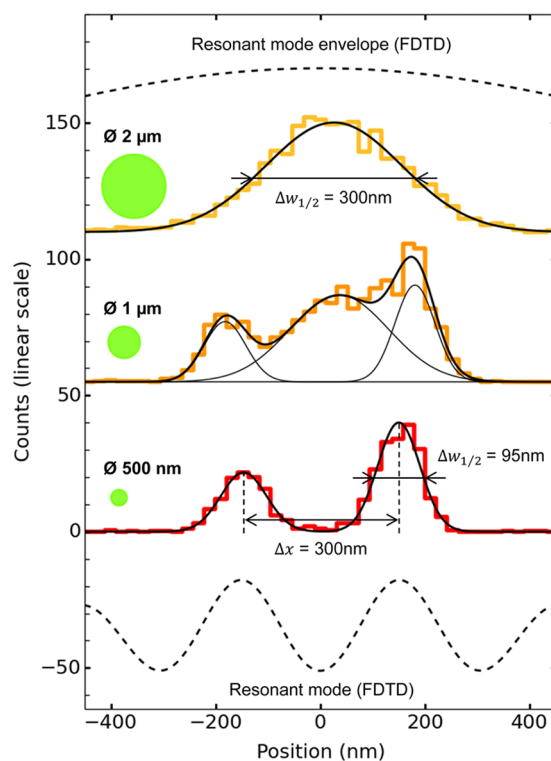

Figure 4. Cross sections along the nanocavity axis of the experimental position probability distributions of trapped microbeads, respectively, 2 μm, 1 μm, and 500 nm in diameter. Whereas the 2 μm bead is sensitive only to the Gaussian envelope of the trapping field, the 500 nm bead is trapped on either one of the two main antinodes of the cavity resonant mode. The 1 μm bead marks the transition between the "averaged" trapping regime (as in the case of the 2 μm bead) and the "proportional" trapping regime (as in the case of the 500 nm bead).

fN·nm^{-1}), the bead's trajectory still covers the whole length of the nanocavity central area. As it can be seen on the cross-section plotted in orange on Figure 4, the probability distribution is non-Gaussian along the nanocavity axis, making it difficult to define an "effective" trap stiffness k_x. Looking more carefully at this cross-section, the position probability distribution can be fitted with the sum of three Gaussian curves. As in the case of the 2 μm bead, the central Gaussian curve, corresponding to a trapping position centered on the cavity, results from the combined effect of the two main antinodes of the resonant mode. However, the presence of two steeper Gaussian curves located on each side of the cavity center means that the 1 μm bead is also influenced independently by each one of these two antinodes. Thus, the 1 μm bead trapping potential map illustrates the transition

between the "averaged" trapping regime, in which two intensity peaks contribute at the same time to trap the microbead at the center of the cavity (as in the case of the 2 μm bead), and another trapping regime, in which the microbead is independently trapped by each intensity peak. This trapping regime is referred to as the "proportional" regime since the trapping potential tends to be proportional to the near-field intensity distribution, as in the Rayleigh approximation. This unpredicted coexistence of two trapping regimes is further evidenced by data showing the nonlinearity between the 1 μm bead trapping potential shape and the trapping laser power (data reported and discussed in Supporting Information).

As shown in Figure 2c, when further decreasing the bead's size to 500 nm, the trapping potential finishes shifting from the "averaged" to the "proportional" regime. The corresponding experimental map reveals indeed two well-separated trapping positions above the nanocavity which clearly correspond to the two main antinodes of the resonant mode. Looking at the cross-section of the position probability distribution plotted in red on Figure 4, the distance between the two central potential wells is about 300 nm, which quantitatively agrees with the relative position of the two most intense antinodes of the cavity resonant mode calculated by 3D FDTD. With full widths at half-maximum of, respectively, 95 and 102 nm, the two Gaussian curves fitting the experimental probability distribution are fully dissociated.

In the case of the 500 nm microbead's trapping, trap stiffnesses higher than in the case of the 2 μm bead are measured, reaching, respectively, $k_x = 2.5 \pm 0.2$ fN·nm^{-1} and $k_y = 8.3 \pm 1.8$ fN·nm^{-1} for the stronger trap (on the right of Figure 2c), and $k_x = 2.1 \pm 0.2$ fN·nm^{-1} and $k_y = 7.2 \pm 0.6$ fN·nm^{-1} for the other one (on the left of Figure 2c). It appears here that the trap stiffness soars (of almost 1 order of magnitude) as the bead size decreases. This behavior is directly related to the transition from one trapping regime to another, resulting from the complex subwavelength shape of the trapping field: Whereas microbeads significantly larger than the spatial variations of the trapping field are sensitive to an average field localization, at the cavity scale, microbeads with a smaller diameter become sensitive to more localized field patterns, at the subwavelength scale.[42] Since subwavelength field patterns generate higher near-field intensity gradients, the last case results in higher lateral optical gradient forces.

Interestingly, two additional trapping positions are also observed on the sides of the nanobeam in Figure 2c. Whereas side walls of the nanocavity are out of reach for both 2 and 1 μm beads for simple geometrical reasons, 500 nm beads are small enough for being trapped by the evanescent field on the edges of the cavity, as shown on Figure 3c. Since the involved surface is now vertical, the microbead centroid is observed at a distance of approximately 250 nm (one microbead's radius) away from each side of the nanobeam. The elongated shapes of these lateral potential wells can be explained by considering the unmodulated evanescent field intensity on the edges of the nanobeam cavity, as it can be seen in Figure 3a. It is worth noticing that this particular side trapping could be further enhanced by optimizing the nanocavity design, as it was recently reported.[43]

The existence of different trapping regimes in optical lattices was already investigated in previous studies,[30−38] where it has mainly found applications in microparticles optical sorting. However, it is here observed and analyzed for the first time in the near-field of a photonic nanostructure that enables high three-dimensional spatial light confinement. Although recent studies based on photonic and plasmonic optical lattices have been reported, none of them has yet focused on the transition between different trapping regimes.[11,12,21,23,44−51] When confronting the present results with previous works (see Supporting Information), it is found that the transition observed here occurs for unexpectedly large particle sizes compared to the intertrap distance. Two elements may be considered as possible reasons for this, both probably contributing at the same time. First, the particular configuration of near-field optical trapping, where only a small part of the trapped microbead interacts with the electromagnetic evanescent field confined close to the surface of the nanocavity. Second, the subwavelength lateral light confinement achieved in the near-field of each antinode of the resonant mode. Be that as it may, the result is that a particle almost twice as big as the intertrap distance can be efficiently trapped in either one of two close but distinct optical traps. This could have interesting repercussions for on-chip optical trapping of micro-objects. An illustration of it is provided hereafter by taking advantage of this result in the field of near-field optical microscopy.

As mentioned above, the "proportional" regime allows for considering the optical trapping potential as proportional to the electromagnetic field intensity: $U_{trap} \propto |E(r)|^2$, at least to a first approximation. Tracking the Brownian motion of a trapped microbead in the "proportional" regime appears therefore as an elegant way to determine the electric near-field intensity distribution of the nanocavity with a subwavelength resolution. We have chosen here to refer to this original near-field microscopy technique as optofluidic near-field optical microscopy. More quantitatively, considering the experimental results shown in Figure 4, the use of a 500 nm bead as fluorescent microprobe enables to resolve two intensity patterns separated by a distance of $\lambda/5$ with a pixel size of a few tens of nanometers. In the experimental scheme depicted here, such a subwavelength resolution relies not only on the much localized interaction between the microsphere and the evanescent field, but also on the fluorescence of the bead. Fluorescence enables indeed to decouple the actual observation wavelength (about 510 nm) from the trapping wavelength (1550 nm), thereby operating an indirect conversion of the infrared evanescent waves into visible propagative waves which can be easily observed with a standard microscope and a moderate numerical aperture objective.

Nonetheless, although the subwavelength resolution is established, one can wonder why only the two central antinodes of the cavity resonant mode appear on the experimental near-field potential image. The microbead being stuck on the two main intensity peaks actually means that the optical trap is too efficient for allowing the bead to move around over the whole cavity surface. In other words, the trapping potential is too deep for the bead to escape from the two main potential wells and explore the whole nanocavity near-field. The thermal energy of the bead, that is, the temperature, acts indeed as a maximum threshold restricting the amplitude of the bead's motion inside the trap. Thus, considering a bead with a given thermal energy, the trapping potential has to be flattened so that the bead can statistically explore a larger area.

This statement was experimentally verified by mapping the potential of a weaker optical trap obtained with a lower input laser power. As expected, the bead's motion was observed to cover a larger extent of the nanocavity surface, allowing for a wider field of view. Most notably, the cross-section of the

trapping potential plotted on Figure 5b now reveals four antinodes of the cavity resonant mode, where only two were
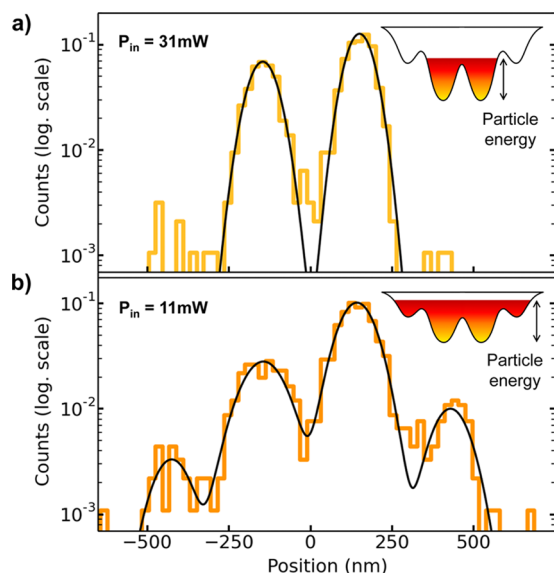

Figure 5. Cross sections along the nanocavity axis of the experimental trapping potential maps obtained by tracking a trapped 500 nm bead (a) before and (b) after loosening the optical trap by decreasing the laser power. The experimental results are fitted with harmonic potential wells. As depicted in the insets, lowering the depth of the potential well allows for a trapped particle with a given energy to access a larger area of the trap.

visible before loosening the trap (Figure 5a). However, this comes with a decreased contrast of the final near-field image since the trapped bead tends to more often get over the barriers separating the different potential wells. From a practical point of view, it also means that the microbead is more inclined to escape from the optical trap during the measurement. The microbead escape rate should yet be kept low enough to give the bead enough time for covering uniformly the whole area of interest during the acquisition time. As a consequence, the trapping potential depth should be considered as a sensitivity threshold that can be adjusted to some extent to balance the near-field image contrast.

CONCLUSION

We have reported in this paper on the experimental description of the trapping potential experienced by polystyrene microbeads in the near-field of a silicon nanobeam cavity. A quantitative analysis of the influence of the bead's size and the input laser power on the trapping potential shape and the "effective" trap stiffness has been also provided. By gradually decreasing the size of the trapped microbeads, we were able to explore the transition between the "averaged" and the "proportional" trapping regimes in the near-field of a photonic nanostructure. Evidence has been made that, unlike in the case of previously investigated optical lattice configurations, this transition interestingly occurs for unexpectedly large particle sizes compared to the intertrap distance. More particularly, it has been found that the nanopatterns of the nanocavity resonant mode clearly appear in the trapping potential map of a 500 nm diameter bead. Those results bring us to envisage optofluidic near-field optical microscopy as an original thermally driven near-field optical microscopy technique, much simpler to implement than conventional scanning probe microscopy techniques,[52,53] aiming at revealing the optical near-field of nanostructures.

ASSOCIATED CONTENT

Ⓢ Supporting Information

The Supporting Information is available free of charge on the ACS Publications website at DOI: 10.1021/acsphotonics.5b00353.

Position distributions obtained from particle tracking; additional data and discussion about the trapping potential of a 1 μm bead trapped at different input laser powers; data taken from the literature and discussion about the critical intertrap distance/particle's size ratio corresponding to the transition between the different trapping regimes (PDF).

AUTHOR INFORMATION

Corresponding Author

*E-mail: benoit.cluzel@u-bourgogne.fr.

Present Address

⊥ICFO-Institut de Ciences Fotoniques, Mediterranean Technology Park, 08860 Castelldefels, Barcelona, Spain (C.R.).

Notes

The authors declare no competing financial interest.

REFERENCES

(1) Ashkin, A. Acceleration and Trapping of Particles by Radiation Pressure. *Phys. Rev. Lett.* **1970**, *24*, 156−159.

(2) Neuman, K. C.; Block, S. M. Optical Trapping. *Rev. Sci. Instrum.* **2004**, *75*, 2787−2809.

(3) Bowman, R. W.; Padgett, M. J. Optical Trapping and Binding. *Rep. Prog. Phys.* **2013**, *76*, 026401.

(4) Kawata, S.; Tani, T. Optically Driven Mie Particles in an Evanescent Field along a Channeled Waveguide. *Opt. Lett.* **1996**, *21*, 1768−1770.

(5) Daly, M.; Sergides, M.; Nic Chormaic, S. Optical Trapping and Manipulation of Micrometer and Submicrometer Particles. *Laser Photon. Rev.* **2015**, *9*, 309−329.

(6) Erickson, D.; Serey, X.; Chen, Y.-F.; Mandal, S. Nanomanipulation Using near Field Photonics. *Lab Chip* **2011**, *11*, 995−1009.

(7) Mandal, S.; Serey, X.; Erickson, D. Nanomanipulation Using Silicon Photonic Crystal Resonators. *Nano Lett.* **2010**, *10*, 99−104.

(8) Renaut, C.; Dellinger, J.; Cluzel, B.; Honegger, T.; Peyrade, D.; Picard, E.; de Fornel, F.; Hadji, E. Assembly of Microparticles by Optical Trapping with a Photonic Crystal Nanocavity. *Appl. Phys. Lett.* **2012**, *100*, 101103.

(9) Descharmes, N.; Dharanipathy, U. P.; Diao, Z.; Tonin, M.; Houdré, R. Single Particle Detection, Manipulation and Analysis with Resonant Optical Trapping in Photonic Crystals. *Lab Chip* **2013**, *13*, 3268−3274.

(10) Van Leest, T.; Caro, J. Cavity-Enhanced Optical Trapping of Bacteria Using a Silicon Photonic Crystal. *Lab Chip* **2013**, *13*, 4358−4365.

(11) Jing, P.; Wu, J.; Lin, L. Y. Patterned Optical Trapping with Two-Dimensional Photonic Crystals. *ACS Photonics* **2014**, *1*, 398−402.

(12) Milord, L.; Gerelli, E.; Jamois, C.; Harouri, a; Chevalier, C.; Viktorovitch, P.; Letartre, X.; Benyattou, T. Engineering of Slow Bloch Modes for Optical Trapping Engineering of Slow Bloch Modes for Optical Trapping. *Appl. Phys. Lett.* **2015**, *106*, 121110.

(13) Renaut, C.; Cluzel, B.; Dellinger, J.; Lalouat, L.; Picard, E.; Peyrade, D.; Hadji, E.; de Fornel, F. On Chip Shapeable Optical Tweezers. *Sci. Rep.* **2013**, *3*, 2290.

(14) Pin, C.; Cluzel, B.; Renaut, C.; Peyrade, D.; Picard, E.; Hadji, E.; de Fornel, F. Optofluidic Taming of a Colloidal Dimer with a Silicon Nanocavity. *Appl. Phys. Lett.* **2014**, *105*, 171108.

(15) Chen, Y.-F.; Serey, X.; Sarkar, R.; Chen, P.; Erickson, D. Controlled Photonic Manipulation of Proteins and Other Nanomaterials. *Nano Lett.* **2012**, *12*, 1633−1637.

(16) Lin, S.; Zhu, W.; Jin, Y.; Crozier, K. B. Surface-Enhanced Raman Scattering with Ag Nanoparticles Optically Trapped by a Photonic Crystal Cavity. *Nano Lett.* **2013**, *13*, 559−563.

(17) Lin, S.; Crozier, K. B. Trapping-Assisted Sensing of Particles and Proteins Using on-Chip Optical Microcavities. *ACS Nano* **2013**, *7*, 1725−1730.

(18) Juan, M. L.; Righini, M.; Quidant, R. Plasmon Nano-Optical Tweezers. *Nat. Photonics* **2011**, *5*, 349−356.

(19) Righini, M.; Volpe, G.; Girard, C.; Petrov, D.; Quidant, R. Surface Plasmon Optical Tweezers: Tunable Optical Manipulation in the Femtonewton Range. *Phys. Rev. Lett.* **2008**, *100*, 186804.

(20) El Eter, A.; Hameed, N. M.; Baida, F. I.; Salut, R.; Filiatre, C.; Nedeljkovic, D.; Atie, E.; Bole, S.; Grosjean, T. Fiber-Integrated Optical Nano-Tweezer Based on a Bowtie-Aperture Nano-Antenna at the Apex of a SNOM Tip. *Opt. Express* **2014**, *22*, 10072−10080.

(21) Roxworthy, B. J.; Toussaint, K. C. Femtosecond-Pulsed Plasmonic Nanotweezers. *Sci. Rep.* **2012**, *2*, 660.

(22) Berthelot, J.; Aćimović, S. S.; Juan, M. L.; Kreuzer, M. P.; Renger, J.; Quidant, R. Three-Dimensional Manipulation with Scanning near-Field Optical Nanotweezers. *Nat. Nanotechnol.* **2014**, *9*, 295−299.

(23) Tanaka, Y.; Kaneda, S.; Sasaki, K. Nanostructured Potential of Optical Trapping Using a Plasmonic Nanoblock Pair. *Nano Lett.* **2013**, *13*, 2146−2150.

(24) Pang, Y.; Gordon, R. Optical Trapping of a Single Protein. *Nano Lett.* **2012**, *12*, 402−406.

(25) Kotnala, A.; Gordon, R. Double Nanohole Optical Tweezers Visualize Protein p53 Suppressing Unzipping of Single DNA-Hairpins. *Biomed. Opt. Express* **2014**, *5*, 1886−1894.

(26) Berg-Sørensen, K.; Flyvbjerg, H. Power Spectrum Analysis for Optical Tweezers. *Rev. Sci. Instrum.* **2004**, *75*, 594.

(27) Phillips, D. B.; Padgett, M. J.; Hanna, S.; Ho, Y.-L. D.; Carberry, D. M.; Miles, M. J.; Simpson, S. H. Shape-Induced Force Fields in Optical Trapping. *Nat. Photonics* **2014**, *8*, 400−405.

(28) Jun, Y.; Tripathy, S. K.; Narayanareddy, B. R. J.; Mattson-Hoss, M. K.; Gross, S. P. Calibration of Optical Tweezers for In Vivo Force Measurements: How Do Different Approaches Compare? *Biophys. J.* **2014**, *107*, 1474−1484.

(29) Schein, P.; Kang, P.; O'Dell, D.; Erickson, D. Nanophotonic Force Microscopy: Characterizing Particle−Surface Interactions Using Near-Field Photonics. *Nano Lett.* **2015**, *15*, 1414−1420.

(30) Šiler, M.; Zemánek, P. Parametric Study of Optical Forces Acting upon Nanoparticles in a Single, or a Standing, Evanescent Wave. *J. Opt.* **2011**, *13*, 044016.

(31) Zemánek, P.; Jonás, A.; Liska, M. Simplified Description of Optical Forces Acting on a Nanoparticle in the Gaussian Standing Wave. *J. Opt. Soc. Am. A* **2002**, *19*, 1025−1034.

(32) Čižmár, T.; Garcés-Chávez, V.; Dholakia, K.; Zemánek, P. Optical Conveyor Belt for Delivery of Submicron Objects. *Appl. Phys. Lett.* **2005**, *86*, 174101.

(33) Ricárdez-Vargas, I.; Rodríguez-Montero, P.; Ramos-García, R.; Volke-Sepúlveda, K. Modulated Optical Sieve for Sorting of Polydisperse Microparticles. *Appl. Phys. Lett.* **2006**, *88*, 121116.

(34) Čižmár, T.; Šiler, M.; Šerý, M.; Zemánek, P.; Garcés-Chávez, V.; Dholakia, K. Optical Sorting and Detection of Submicrometer Objects

in a Motional Standing Wave. *Phys. Rev. B: Condens. Matter Mater. Phys.* **2006**, *74*, 035105.

(35) Jákl, P.; Čižmár, T.; Šerý, M.; Zemánek, P. Static Optical Sorting in a Laser Interference Field. *Appl. Phys. Lett.* **2008**, *92*, 161110.

(36) Mu, W.; Li, Z.; Luan, L.; Spalding, G. C.; Wang, G.; Ketterson, J. B. Force Measurement on Microspheres in an Optical Standing Wave. *J. Opt. Soc. Am. B* **2008**, *25*, 763−767.

(37) Shilkin, D. a.; Lyubin, E. V.; Soboleva, I. V.; Fedyanin, A. Trap Position Control in the Vicinity of Reflecting Surfaces in Optical Tweezers. *JETP Lett.* **2014**, *98*, 644−647.

(38) Jákl, P.; Arzola, A. V.; Šiler, M.; Chvátal, L.; Volke-Sepúlveda, K.; Zemánek, P. Optical Sorting of Nonspherical and Living Microobjects in Moving Interference Structures. *Opt. Express* **2014**, *22*, 29746−29760.

(39) Velha, P.; Rodier, J. C.; Lalanne, P.; Hugonin, J. P.; Peyrade, D.; Picard, E.; Charvolin, T.; Hadji, E. Ultracompact Silicon-on-Insulator Ridge-Waveguide Mirrors with High Reflectance. *Appl. Phys. Lett.* **2006**, *89*, 171121.

(40) Florin, E.-L.; Pralle, A.; Stelzer, E. H. K.; Hörber, J. K. H. Photonic Force Microscope Calibration by Thermal Noise Analysis. *Appl. Phys. A: Mater. Sci. Process.* **1998**, *66*, S75−S78.

(41) Chenouard, N.; Smal, I.; de Chaumont, F.; Maška, M.; Sbalzarini, I. F.; Gong, Y.; Cardinale, J.; Carthel, C.; Coraluppi, S.; Winter, M.; Cohen, A. R.; Godinez, W. J.; Rohr, K.; Kalaidzidis, Y.; Liang, L.; Duncan, J.; Shen, H.; Xu, Y.; Magnusson, K. E. G.; Jaldén, J.; Blau, H. M.; Paul-Gilloteaux, P.; Roudot, P.; Kervrann, C.; Waharte, F.; Tinevez, J.-Y.; Shorte, S. L.; Willemse, J.; Celler, K.; van Wezel, G. P.; Dan, H.-W.; Tsai, Y.-S.; Ortiz de Solórzano, C.; Olivo-Marin, J.-C.; Meijering, E. Objective Comparison of Particle Tracking Methods. *Nat. Methods* **2014**, *11*, 281−289.

(42) Barth, M.; Benson, O. Manipulation of Dielectric Particles Using Photonic Crystal Cavities. *Appl. Phys. Lett.* **2006**, *89*, 253114.

(43) Lin, P.-T.; Lu, T.-W.; Lee, P.-T. Photonic Crystal Waveguide Cavity with Waist Design for Efficient Trapping and Detection of Nanoparticles. *Opt. Express* **2014**, *22*, 6791−6800.

(44) Grujic, K.; Hellesø, O. G. Dielectric Microsphere Manipulation and Chain Assembly by Counter-Propagating Waves in a Channel Waveguide. *Opt. Express* **2007**, *15*, 6470−6477.

(45) Grigorenko, a. N.; Roberts, N. W.; Dickinson, M. R.; Zhang, Y. Nanometric Optical Tweezers Based on Nanostructured Substrates. *Nat. Photonics* **2008**, *2*, 365−370.

(46) Roxworthy, B. J.; Ko, K. D.; Kumar, A.; Fung, K. H.; Chow, E. K. C.; Liu, G. L.; Fang, N. X.; Toussaint, K. C. Application of Plasmonic Bowtie Nanoantenna Arrays for Optical Trapping, Stacking, and Sorting. *Nano Lett.* **2012**, *12*, 796−801.

(47) Roxworthy, B. J.; Toussaint, K. C. Plasmonic Nanotweezers: Strong Influence of Adhesion Layer and Nanostructure Orientation on Trapping Performance. *Opt. Express* **2012**, *20*, 9591−9603.

(48) Chen, K. Y.; Lee, A. T.; Hung, C. C.; Huang, J. S.; Yang, Y. T. Transport and Trapping in Two-Dimensional Nanoscale Plasmonic Optical Lattice. *Nano Lett.* **2013**, *13*, 4118−4122.

(49) Jaquay, E.; Martínez, L. J.; Huang, N.; Mejia, C. a; Sarkar, D.; Povinelli, M. L. Light-Assisted, Templated Self-Assembly of Gold Nanoparticle Chains. *Nano Lett.* **2014**, *14*, 5184−5188.

(50) Soltani, M.; Lin, J.; Forties, R. a; Inman, J. T.; Saraf, S. N.; Fulbright, R. M.; Lipson, M.; Wang, M. D. Nanophotonic Trapping for Precise Manipulation of Biomolecular Arrays. *Nat. Nanotechnol.* **2014**, *9*, 448−452.

(51) Huang, N.; Martínez, L. J.; Jaquay, E.; Nakano, A.; Povinelli, M. L. Optical Epitaxial Growth of Gold Nanoparticle Arrays. *Nano Lett.* **2015**, *15*, 5841−5845.

(52) Lalouat, L.; Cluzel, B.; de Fornel, F.; Velha, P.; Lalanne, P.; Peyrade, D.; Picard, E.; Charvolin, T.; Hadji, E. Subwavelength Imaging of Light Confinement in High-Q/small-V Photonic Crystal Nanocavity. *Appl. Phys. Lett.* **2008**, *92*, 111111.

(53) Huang, F.; Ananth Tamma, V.; Mardy, Z.; Burdett, J.; Kumar Wickramasinghe, H. Imaging Nanoscale Electromagnetic Near-Field Distributions Using Optical Forces. *Sci. Rep.* **2015**, *5*, 10610.